Chemical Science

Accepted Manuscript

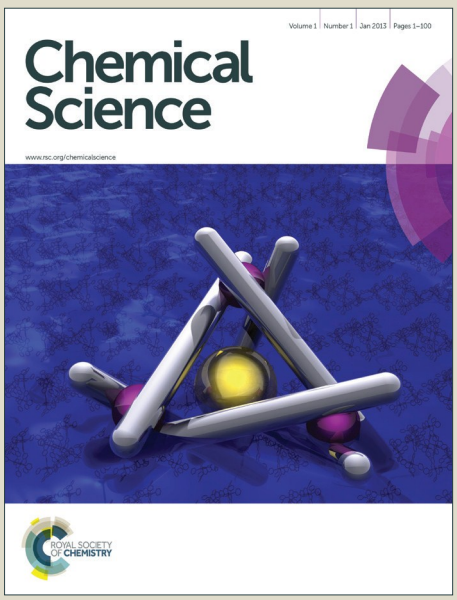

ROYAL SOCIETY OF CHEMISTRY

www.rsc.org/chemicalscience

Journal Name

ARTICLE

Nucleic acid-selective light-up fluorescent biosensors for ratiometric two-photon imaging the viscosity of live cells and tissues

Received 00th January 20xx,
Accepted 00th January 20xx

DOI: 10.1039/x0xx00000x

www.rsc.org/

Dandan Li,[a]† Xiaohe Tian,[b]† Aidong Wang,[c] Lijuan Guan,[d] Jun Zheng,[a] Fei Li,[a] Shengli Li,[a] Hongping Zhou,[a] Jieying Wu,[a] Yupeng Tian*[a]

Rational designing specific ratiometric viscosity probes with small molecular weight is a challenge in practical biotechnology applications. Herein two novel water-soluble, small molecular ratiometric probes, bearing N-methyl benzothiazolium moiety (DSF and DBF), are designed for two-photon fluorescent imaging as a functional of local viscosity. The dye DSF, a light-up fluorescent probe, was sensitive to local viscosity and selectively stains nuclear DNA, which can inspect asynchronous cells under confocal microscopy. While the dye DBF as a molecular rotor displays strong fluorescence enhancement in viscous media or binding to RNA. It exhibits dual absorption and emission as well, and only the red emission is markedly sensitive to viscosity changes, providing a ratiometric response and selectively imaging nucleolic and cytosolic RNA. Interestingly it is showed, for the first time, that the intracellular targeting and localization (DNA and RNA) of the two dyes are entirely realized simply by modifying the substituent attached onto the benzothiazolium.

Introduction

Insight into the character of each component in a cellular system and their complex biological functions and processes has attracted increasing attention, better understanding of the selective staining/imaging of specific cellular organelles is therefore of paramount importance.[1] Since nucleic acid (NA) including DNA and RNA is the major sources to store, duplicate and transfer the genetic information in all eukaryotic cells,[2,3] design tools in nucleic acid imaging have become of great interest.[4-7] Whereas commercial nuclear imaging agents[8] such as DAPI, Hoechst 33342 (DNA) and SYTO-Select (RNA) probe, which require ultraviolet light as excitation source, resulting in significant autofluorescence and extensive photon toxicity.[9,10] An attractive approach for the selective detection of NA in living samples is ratiometric imaging with two-photon microscopy (TPM). The former offers quantitatively measurement and avoids most of the interferences from microenvironments, the latter gives deeper tissue penetration and autofluorescence free background.[11-18] However, ratiometric two-photon absorption molecules generally possess large π-conjugated system, resulting in relatively big molecular weight and involve extensive synthesis procedures.[19-24] Therefore, NA-specific ratiometric two-photon excited fluorescence (TPEF) probes with optimized two-photon action cross-section (Φδ) and appropriate biocapability (e.g. aqueous solubility, membrane permeability) are next ideal image system.

Additionally, viscosity strongly influences intracellular substances transportation, biomacromolecules interactions, and reactive metabolites diffusion in live cells,[25] and consequently abnormal viscosity fluxion strongly reflect many diseases and malfunctions.[26-30] In recent years, ''molecular rotors'', the microviscosity-targeted fluorescent sensors have gradually emerged with the application of fluorescence technology.[31-36] Nevertheless, these sensors are unable to quantitatively determine intracellular microviscosity or its variations due to the influence of experimental and instrumental factors. Therefore, novel molecular rotors with dual emission maxima capable of quantifying viscosity[37-41] in living samples and avoids most of the interferences are indeed in demand.

Considering above, two water-soluble small organic molecules with optimized two-photon action cross-section were designed. The introduction of N-methyl benzothiazolium moiety (as a acceptor A) and the ease of modifying the substituent attached onto the benzothiazolium results in strong and concomitant optimization of both optical performances and NA binding parameters. 2-(Methylamino)ethanol unit act as a donor (D) and its HO- group

[a] Department of Chemistry, Anhui University, Hefei, China.
[b] School of life science, Anhui University, Hefei, China.
[c] Huangshan University, Huangshan, China.
[d] Department of Chemistry, University College London, London, UK.
† These authors contributed equally.
Electronic Supplementary Information (ESI) available: The detailed synthetic processes, fully characterizations of the two dyes. The crystal structural and DNA binding information of DSF. The water solubility, PH effect, cytotoxicity and photostability of DSF and DBF. See DOI: 10.1039/x0xx00000x

should trend to form strong hydrogen bonding with the other polar molecules around its microenvironment. It was found that the minor modification of the substituent attached onto the benzothiazolium significantly alters the final subcellular destination. Consequently, this led to the identification of two novel 2PEF probes called DSF and DBF have the high affinity binding to nuclear DNA and intracellular RNA, respectively. Importantly, inside living cells and tissues the viscosity changes, showing some regional difference, can be clearly observed by ratiometric two-photon imaging using such two probes. This is the first time that two 2PA fluorescent agents, which also offer in-situ intracellular viscosity quantitatively, have been applied to image DNA and RNA in living cells and tissues.

Results and discussion

Experimental

One-Photon Excited Fluorescence (OPEF) response to solvent viscosity. Generally solvents with different polarity influence the wavelengths and quantum yields to some extent. However, as shown in Figure 1 (a, d), the quantum yield (QY) of DSF or DBF was very low in low-viscosity solvents, and apparently was not affected by solvent polarity. On the other hand, DSF and DBF showed a sharp fluorescence enhancement with increasing of the solvent viscosity. As glycerol was gradually added to mixture solvent, the viscosity of the solutions increased from 1.0 cP (water) to approximately 950 cP (99% glycerol), consequently the fluorescence of DSF and DBF increased 19-fold (QY= 0.27) and 16-fold (QY= 0.35) in 99% glycerol, respectively. This is crucial to permit a molecular rotor to reflect environmental viscosity.[42]

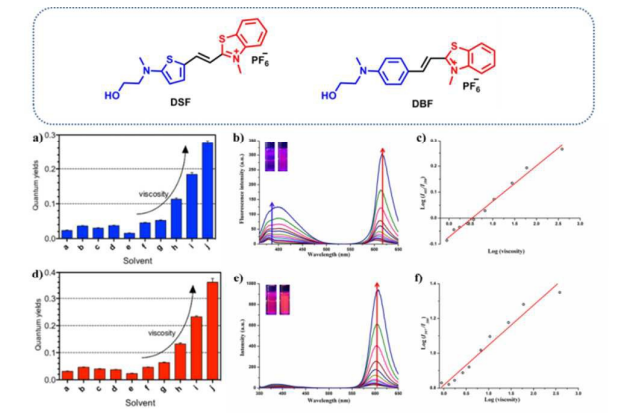

Figure 1. The fluorescence quantum yields of DSF (**a**, λ_{ex} = 560 nm) and DBF (**d**, λ_{ex} = 505 nm) in different solvents: *a*) dichloromethane, *b*) DMSO, *c*) ethanol, *d*) methanol, *e*) water, *f*) water/glycerol (8:2 v/v), *g*) water/glycerol (6:4 v/v), *h*) water/glycerol (4:6 v/v), *i*) water/glycerol (2:8 v/v), *j*) glycerol (99%); Changes in the fluorescence emission spectra of DSF (**b**) and DBF (**e**) as a function of the solvent viscosity (excited at 335 nm). Inset: Photographs taken under UV illumination of DSF and DBF in water (left) and 99% glycerol (right), respectively; The linear response between the log ($I_{605\ nm}/I_{380\ nm}$) for DSF (**c**), log ($I_{597nm}/I_{380\ nm}$) for DBF (**f**) and the log (viscosity) in the water/glycerol solvent (excited at 335 nm), respectively.

To further investigate their utility as molecular rotors to quantifying viscosity, the changes of fluorescence emission spectra for DSF and DBF as a function of the solvent viscosity were performed. As illustrated in **Figure S3**, DSF exhibits two emission bands in aqueous solution. The red-emission band (λ_{em}(red)=605 nm) rose much faster than the blue-emission band (λ_{em}(blue)= 380 nm) as the viscosity of solution was increased (**Figure 1b**). In addition, the logarithm of the fluorescence ratio thereof ($I_{605\ nm}/I_{380\ nm}$) has a linear relationship with that of the viscosity (η) of the solution, which is as expected from the Förster–Hoffmann equation:[43]

$$\log I_f = C + x \log \eta$$

Where *C* is a concentration that is temperature-dependent, and *x* is a dye-dependent constant. Therefore, log ($I_{605\ nm}/I_{380\ nm}$) of DSF and logη were fitted accordingly (**Figure 1c**, R^2 = 0.99, the slope *x* = 0.14). In addition, similar to DSF, DBF possesses a unique spectral character, with two emission peaks (such as λ_{em} 380 and 597 nm in water, **Figure S3**). Most importantly, only the red emission of DBF responded significantly to the viscosity of the solvent. As shown in **Figure 1e**, with increasing proportions of glycerol in the mixture solvent, the red fluorescence intensity at 597 nm increased sensitively with viscosity of the solvents. The blue emission at 380 nm, however, gave only very small responses. This permits ratiometric changes with a linear relationship between log(I_{597}/I_{380}) and *log η*, which is fitted by the Förster–Hoffmann equation, R^2 of the linear relation increases in the water-glycerol system (**Figure 1f**) was 0.96, and the slope *x* was 0.23. It indicated that DSF and DBF could be applied as ratiometric sensors to quantitatively detect the solution viscosity.

Two-Photon absorption (TPA) response to solvent viscosity. Stilbazolium salts with D-π-A molecular configuration have been reported to have two-photon properties.[44-46] As shown in **Figure 2**, the two-photon absorption spectra of DSF and DBF increased significantly with a rise in solvent viscosity. The two-photon action cross-section ($\Phi\delta$) at 720 nm of DSF increased from 5.0 (water) to 75.6 GM (99% glycerol) and the $\Phi\delta$ at 800 nm of DBF increased from 9.0 (water) to 98.8 GM (99% glycerol), respectively (1 GM=10^{-50} cm^4 s $photon^{-1}$). Their reasonable two-photon action cross-sections are the attractive features for their utility as biological probes.

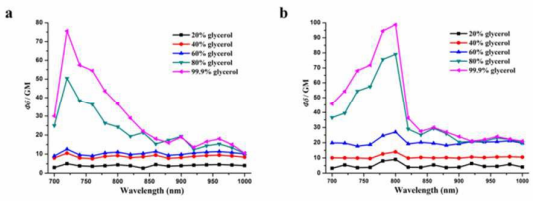

Figure 2. Two-photon (TP) action cross-section spectra of DSF (left, 0.1 mM) and DBF (right, 0.1 mM) in solvents of varying viscosity. TP excitation: 700-1000 nm.

The cellular uptake properties of DSF and DBF. Considering the comprehensive merits of the dyes, biological imaging application of DSF and DBF were carried out using HepG2 cells (liver hepatocellular carcinoma) as a model. Initially their cytotoxicity and photon resistance abilities were evaluated via standard MTT assay and photon bleaching experiments (**Figure S7**). Above results suggested the noninvasiveness at even high concentration (25μM) and strong photon resistance against laser irradiation (150s), giving feasibility for further studies in living samples.

Cell localization of DSF: A DNA-specific luminescent cellular imaging agent. Cell-staining experiments using two-photon confocal microscopy showed that DSF (10 μM, 30 min) could readily enter living HepG2 cells effectively and predominantly emission is apparently observed from the cell nucleis (**Figure 3a**). Furthermore, DSF visualizes characteristic structural changes in nuclear DNA as cells progress through the cell cycle. As showed in higher resolution micrographs (**Figure 3b**) of single cell, when asynchronous cells are imaged, the majority of labelled cells are interphase but cells undergoing mitotic phases are also clearly observed. Notably, cell under goes interphase with dense chromosomes (**Figure 3a**, white arrows) obviously displayed brighter signal as an indication of local DNA viscosity. To the best of our knowledge, the DNA-specific 2PA luminescent cellular imaging probes, which can inspect asynchronous cells by cell imaging, are extremely rare.[47,48]

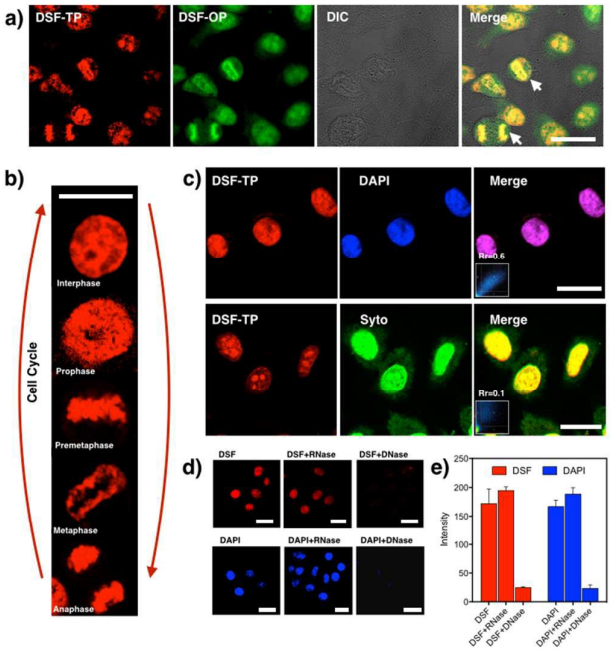

Figure 3. Fluorescent images of living cells by DSF. **a**) One and two-photon excitation were at 488 and 720 nm, respectively: OPM image of DSF (580-620 nm), TPM image of DSF (590-630 nm); **b**) Asynchronous cell imaging shows mitotic cells stained by DSF visualizing chromosome aggregation through progression of mitosis; **c**) Co-staining of DSF (red, TPM: λ_{ex} = 720 nm) with DNA-specific dye DAPI (blue) and general nucleic acid dye SYTO 9 (green); **d**) DNase and RNase digest experiments of DSF (TPM: λ_{ex} = 720 nm) and DAPI (shown as comparison experiments); **e**) The intensity of fluorescent images for DNase and RNase digest experiments. Scale bar: 20 μm.

To establish the precise intracellular localization of DSF, co-staining experiments were performed. Incubation of HepG2 cells with DSF and co-staining with the membrane-permeable DAPI, a DNA minor-groove binder, shows strong co-localization of the two emission signals (**Figure 3c**, Pearson's correlation coefficient: Rr = 0.60). Conversely, co-staining with SYTO 9, a general nucleic acid stain, shows a clear difference in localization (Rr = 0.10). In addition, deoxyribonuclease (DNase) and ribonuclease (RNase) digest experiments were also performed (**Figure 3d** and **3e**) to identify the stained species by DSF in the nuclear, while DAPI was also tested as control. Upon treatment with RNase, no significant loss of fluorescence in the nuclear occurred for DSF. By contrast, after DNase digestion, the nuclear fluorescence signals of DSF were completely lost. DSF exhibited a similar behavior in the digest experiment with DAPI, indicating that nuclear fluorescence originated from the binding of CP with DNA in the nuclear. DNase/RNase digest experiments and co-staining with other commercially available fluorescent nuclear stains reveals that DSF is clearly targeting nuclear DNA in live cells.

Cell localization of DBF: imaging of RNA-rich nucleolus and RNA in cytoplasm. In a parallel experiment, a living cell sample was incubated with 10 μM DBF for 30 min. As shown in **Figure S10A**, the green fluorescence mainly localizes at the cytoplasm and nucleoli accompanied with faint nuclei distribution. In addition, two-photon microscopy has revolutionized the biological sciences by enabling non-invasive, high-resolution imaging of living samples in real time. Therefore, to confirm the fluorescence spots observed in the nucleolus, the two-photon fluorescence images and DIC pictures were compared **Figure S10B**, and bright fluorescence spots just coincide with nucleoli, the densest and phase-dark region of the nucleus. In addition, co-staining experiments were performed as well (**Figure 4a**), the DBF signal showed strong overlap with SYTO 9 (Rr = 0.76). Conversely, the colocaolization profile showed minimal overlapping between DBF and DAPI (Rr = 0.34).

As we all know, the nucleolus contains abundant RNAs and proteins, especially ribosomal RNA and ribosomal proteins. To investigate the selectivity for RNA of DBF in cells, the digest test of ribonuclease (RNase), which only hydrolyzes the RNA in the cell and does not influence the DNA, was performed (**Figure 4b**). The only commercial RNA probe, SYTO RNA-Select, was also used as control. From the **Figure 4b**, as the same as SYTO RNA-Select, in contrast to the untreated samples the fluorescence of DBF in cytoplasm and nucleoli dramatically diminished and tended to redistribute to the nucleoli. In addition, upon treatment with DNase, no significant loss of fluorescence in the nuclear occurred for DBF and SYTO RNA-

Select (**Figure 4c**). The result indicates DBF can selectively stain RNA in the nucleolus and cytoplasm, which would display to advantage greatly in the observation of RNA content and distribution and the visualization of nucleolus-related events.

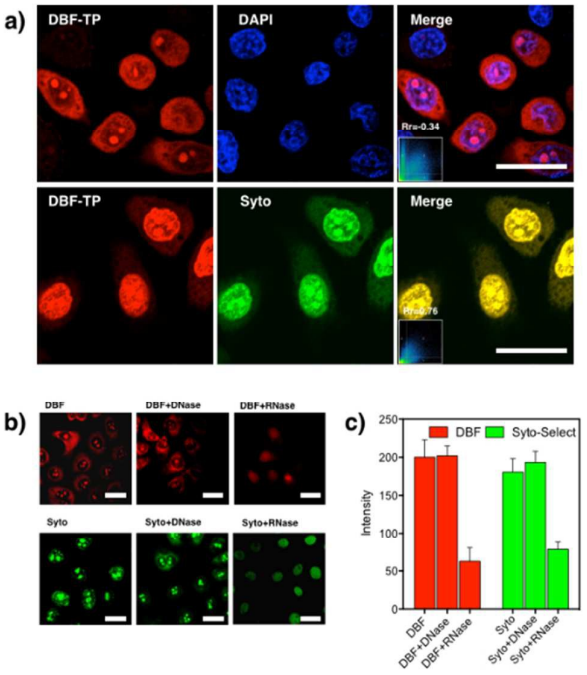

Figure 4. **a**) Co-staining of DBF (red, TPM: λ_{ex} = 800 nm) with DNA-specific dye DAPI (blue) and general nucleic acid dye SYTO 9 (green); **b**) DNase and RNase digest experiments of DBF (TPM: λ_{ex} = 800 nm) and SYTO 9; **e**) The intensity of fluorescent images for DNase and RNase digest experiments. Scale bar: 20 μm.

Ratiometric two-photon fluorescence cell and tissue imaging. Since DSF and DBF could be applied with the fluorescence-enhancement method that senses the viscosity change, the two NA sensors with two emission peaks can be also applied to the ratiometric fluorescence imaging of viscosity in live cells. Excited at 720 nm for DSF and 800 nm for DBF, the fluorescence images were obtained by collecting the blue emission of (375–450 nm) (green channel) and the red emission of (570–650 nm) (red channel) (**As shown in Figure 5**). The ratio image ($I_{605\ nm}/I_{380\ nm}$) of DSF and ($I_{597\ nm}/I_{380\ nm}$) clearly displayed the distribution of viscosity in the cells (left, **Figure 6**). In addition, due to their 2PA property, we further investigated the application of these sensors in thick tissue imaging (>200μm) in *ex vivo*. The fresh rat liver slice incubated with 10 μM DSF or DBF for 30 min not only showed the DNA/RNA labeling but also offered viscosity distribution (**Figure 6**, right). The "blue" regions, indicating the viscosity is less than 100 cP, the "green" imaging areas represent an intermediate viscosity of cell and tissue slice (100–500 cP). In some small intracellular red zones indicate high viscosity (about 900 cP) in living samples.

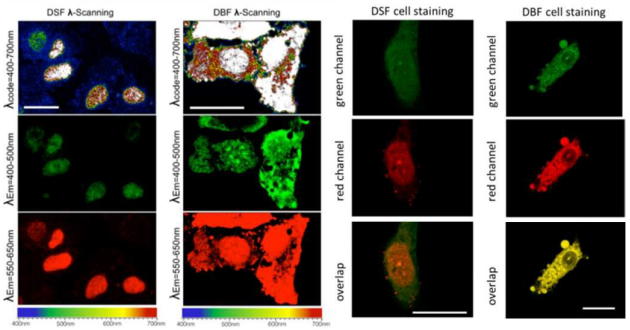

Figure 5. Live HepG2 cells staining with DSF (10 μM, 30 min incubation, excited at 720 nm) and DBF (10 μM, 30 min incubation excited at 800 nm): green channel (375–450 nm), red channel (570–650 nm). Scale bar: 20 μm.

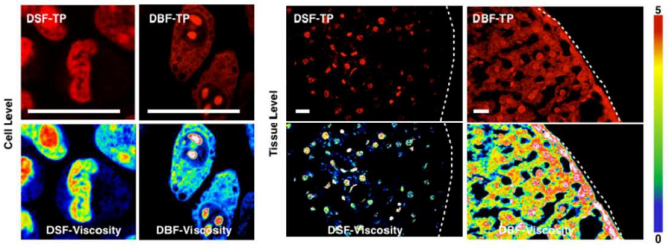

Figure 6. Live HepG2 cells and fresh rat liver slice staining with DSF (10 μM, 30 min incubation, excited at 720 nm) and DBF (10 μM, 30 min incubation excited at 800 nm), red channel (570-650 nm), the ratio image of DSF and DBF obtained by the ImageJ software.

Above results showed that the two NA sensors as two-photon ratiometric rotors could be used to inspect viscosity changes *in vitro* and *ex vivo* by ratiometric two-photon imaging. Additionally, the two rotors with dual emission maxima capable of quantifying viscosity in cells and tissues, which avoid most of the interferences from the fluid optical properties, dye concentration, and other experimental or instrumental factors.

Possible influencing factors on targeting and localization properties. To further investigate the DSF preference to DNA and DBF preference to RNA *in vitro*, the interactions of dyes DSF and DBF with numerous substances in the nucleus, including various amino acids, peptides, deoxyribonucleotide (dNTP), proteins, DNA, and RNA, were examined by absorption and fluorescence spectra. As shown in **Figure S11** and **Table S3**, the observation of hypochromism in the absorption spectra are due to the stacking interactions between the aromatic ring and the base pairs of DNA.[49] Meanwhile, the addition of DNA to DSF triggered a pronounced bathochromic effect in absorption spectra and a significant luminescence enhancement ("light-switch" effect, **Figure S11B**) while other biological molecules do not give rise to such effect, which reveal the strong interaction between DSF and DNA, in agreement with the initial cell-staining experiments. In addition, as

Figure S11C shows, upon addition of NA (DNA and RNA), a pronounced bathochromic effect in absorption spectra is observed for DBF, which reveal the strong interaction between DBF and NA. The fluorescence intensity of DBF upon RNA displays a larger fluorescence enhancement than DNA for the same amount of NA (**Figure S11D**). A similar phenomenon for SYTO RNA-Select was also observed in reported works,[50] indicating that DBF and SYTO RNA-Select both have higher response to RNA than to DNA. While the cell-staining experiments indicate DBF selectively stain RNA in cells, and this puzzling state is possibly due to the difference between structure of nucleic acids in solution and their real state in cells and specific interaction between different probes and nucleic acids.[51] Accordingly, the weak emission of DSF and DBF in water can be attributed to the strong interaction of the molecules at excited state with the water environment, which induce the formation of twisting intramolecular charge transfer state, resulting in the increase of nonradiative decay. As for the luminescence enhancement of dyes DSF and DBF binding to NA could be explained by two factors: firstly, the immobilization that reduces non-radiative processes associated to molecular internal rotation around the vinyl bond; secondly, the screening from water once the dyes are inserted inside NA.[52]

Considering DSF and DBF both can bind to DNA, to understand more thoroughly the sequence selectivity of them, we studied them in presence of the polynucleotides poly(dA-dT)$_2$ and poly(dG-dC)$_2$. As shown in the **Figure S12**, the increase in fluorescence of DSF/DBF in the former is higher than the latter which due to the AT display a more negative electrostatic potential as compared to other sequences, which is favorable to cation trapping.[4] On the basis of the data obtained by the above, we conducted molecular modeling calculations[53] on Discovery Studio4.1 (Huangshan University) with duplex DNA fragment (duplex AT-rich DNA, base sequences CTTTTGCAAAAG/CTTTTGCAAAAG). The docking results (**Figure 7**) indicate that DSF and DBF can bind to duplex DNA by intercalating DNA via the hydrogen bonding interactions of nucleobases (prefer to A≡T, which is agreement with the results of fluorescence spectra change of DSF/DBF in polynucleotides poly(dA-dT)$_2$ and poly(dG-dC)$_2$). In addition, as shown in **Table S4**, DSF bind to DNA with higher affinity (lower CDOCKER energy) which might due to DSF interacts with the base pairs of DNA via hydrogen bonds in different directions (**Figure S14**), resulting in the DSF can be inserted inside DNA in stable configuration. While, as shown in **Figure S15**, DBF interacts with the base pairs of DNA by hydrogen bonds in the same direction and in the action of the same force field, the structure of DBF binding to DNA will be twisted.

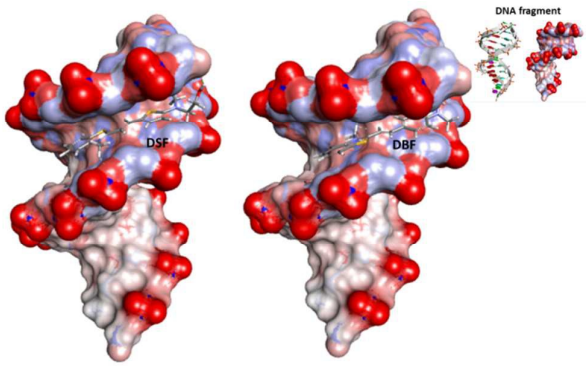

Figure 7. Models obtained after molecular modeling for the interaction of DSF and DBF with DNA fragment. Inset figure: the structure of corresponding DNA fragment.

The knowledge of the interaction mechanism between RNA and fluorescent probes is still not enough compared with the wealth of deeper understanding of DNA biosensors. Besides, compared to the many fluorescent probes imaging DNA, the mechanisms of RNA probes for cell imaging are rarely reported. Molecular Probes Co., which sells various DNA probes such as DAPI, series of Hoechsts, and propidium iodide, only offered a classical commercial RNA probe "SYTO RNA-Select" for imaging RNA in living cells, but its chemical structure has not been described. Although it is not very clear why just by changing the linker thiophene (DSF) to phenyl (DBF) the binding selectivity changes from DNA to RNA. Considering the results of molecular modeling calculations for DBF and DNA fragment, it is tentatively suggested that the difference occurred which may due to the fact that (i) some specificity of intracellular distribution and organization of RNA and DNA molecules can cause a difference in the affinity of dye DSF or DBF to DNA and RNA inside cells. (ii) DBF interacts with the base pairs of RNA by hydrogen bonds in the same direction (similar with DNA binding) and in the action of the same force field, the structure of DBF binding to RNA will be twisted into stable crescent-shape configuration. DBF exhibits much stronger binding affinity toward RNA than DNA in a buffer solution and selectively stains and targets RNA in the cells which might be attributable to crescent-shape molecules with positive charges may prefer binding with RNA.[54,55] As mentioned above, the DSF is clearly targeting nuclear DNA and DBF selectively stain RNA in living cells. The two dyes, because of the ease of modifying the substituent attached onto the thiazole, the intracellular targeting and localization properties are entirely different. These findings suggest that a variation of substituent attached onto the benzothiazolium moiety can greatly vary the binding interaction with NA and thus provide a tool to fine-tune the targeting and localization properties of organic molecules as effective organelle specific TPEF probes.

Conclusions

In summary, two water-soluble small organic ratiometric molecules with optimized two-photon action cross-section were developed. Because of the ease of modifying the substituent attached onto the

benzothiazolium, the targeting and localization properties can be easily tuned and optimized for the organic molecules as effective organelle-specific TPEF probes. The two novel TPEF probes called DSF and DBF binding to nuclear DNA and RNA in the nucleolus and cytoplasm with high affinity, respectively. Importantly, the two unique fluorescent nucleic acid light-up probes as two-photon ratiometric rotors can be used for quantifying and imaging intracellular viscosity in living cells and tissues. Their advantages of exclusive NA-selective staining of living cells, high signal ratio, excitation with NIR light, good photostability, as well as low cytotoxicity at imaging concentration, promise potential applications of DSF and DBF in biological and biomedical research.

Acknowledgements

This work was supported by the National Natural Science Foundation of China (21271004, 51372003, 51432001, 21271003, 51472002), Focus on returned overseas scholar of Ministry of Education of China, the Higher Education Revitalization Plan Talent Project (2013).

Notes and references

1. I. B. Buchwalow and W. Böcker, *Immunohistochemistry: Basics and Methods*, Springer: Berlin, 2010.
2. A. Z. Medvedev, *Adv. Gerontol. Res.*, 1964, **21**, 181-206.
3. J. Brachet, *Prog. Biophys. Mol. Biol.*, 1965, **15**, 95-127.
4. B. Dumat, G. Bordeau, E. Faurel-Paul, F. Mahuteau-Betzer, N. Saettel, G. Metge, C. Fiorini-Debuisschert, F. Charra and M. P. Teulade-Fichou, *J. Am. Chem. Soc*, 2013, **135**, 12697-12706.
5. L. Guo, M. S. Chan, D. Xu, D. Y. Tam, F. Bolze, P. K. Lo and M. S. Wong, *ACS Chem. Biol.*, 2015, **10**, 1171-1175.
6. P. Hanczyc, B. Norden and M. Samoc, *Dalton Trans.*, 2012, **41**, 3123-3125.
7. X. Liu, Y. Sun, Y. Zhang, F. Miao, G. Wang, H. Zhao, X. Yu, H. Liu and W. Y. Wong, *Org. Biomol. Chem.*, 2011, **9**, 3615-3618.
8. Invitrogen Home pages, *www.probes.com and www.invitrogen. com*; R. P. Haugland, *A Guide to Fluorescent Probes and Labelling Technologies*, 10th ed.; Molecular Probes: Eugene, OR, 2005, 397-405.
9. G. P. Pfeifer, Y. H. You and A. Besaratinia, *Mutat. Res.*, 2005, **571**, 19-31.
10. H. M. Kim and B. R. Cho, *Chem Rev*, 2015, **115**, 5014-5055.
11. W. R. Zipfel, R. M. Williams and W. W. Webb, *Nat. Biotechnol.*, 2003, **21**, 1369-377.
12. F. Helmchen and W. Denk, *Nat. Methods*, 2005, **2**, 932-940.
13. R. M. Williams, W. R. Zipfel and W. W. Webb, *Curr. Opin. Chem. Bio.*, 2001, **5**, 603-608.
14. L. Guo and M. S. Wong, *Adv. Mater.*, 2014, **26**, 5400-5428.
15. H. M. Kim, B. H. Jeong, J. Y. Hyon, M. J. An, M. S. Seo, J. H. Hong, K. J. Lee, C. H. Kim, T. Joo, S. C. Hong and B. R. Cho, *J. Am. Chem. Soc.* , 2008, **130**, 4246-4247.
16. X. H. Wang, D. M. Nguyen, C. O. Yanez, L. Rodriguez, H. Y. Ahn, M. V. Bondar and K. D. Belfield, *J. Am. Chem. Soc.* , 2010, **132**, 12237-12239.
17. J. H. Han, S. K. Park, C. S. Lim, M. K. Park, H. J. Kim, H. M. Kim and B. R. Cho, *Chem. Eur. J.*, 2012, **18**, 15246-15249.
18. W. Yang, P. S. Chan, M. S. Chan, K. F. Li, P. K. Lo, N. K. Mak, K. W. Cheah and M. S. Wong, *Chem. Commun.*, 2013, **49**, 3428-3430.
19. K. P. Divya, S. Sreejith, P. Ashokkumar, K. Yuzhan, Q. Peng, S. K. Maji, Y. Tong, H. Yu, Y. Zhao, P. Ramamurthy and A. Ajayaghosh, *Chem. Sci.*, 2014, **5**, 3469-3474.
20. L. Yuan, F. Jin, Z. Zeng, C. Liu, S. Luo and J. Wu, *Chem. Sci.*, 2015, **6**, 2360-2365.
21. C. S. Lim, G. Masanta, H. J. Kim, J. H. Han, H. M. Kim and B. R. Cho, *Journal of the American Chemical Society*, 2011, **133**, 11132-11135.
22. S. K. Bae, C. H. Heo, D. J. Choi, D. Sen, E. H. Joe, B. R. Cho and H. M. Kim, *J. Am. Chem. Soc.*, 2013, **135**, 9915-9923.
23. H. J. Kim, C. H. Heo and H. M. Kim, *J. Am. Chem. Soc.*, 2013, **135**, 17969-17977.
24. L. Zhou, X. Zhang, Q. Wang, Y. Lv, G. Mao, A. Luo, Y. Wu, Y. Wu, J. Zhang and W. Tan, *J. Am. Chem. Soc.*, 2014, **136**, 9838-9841.
25. S. T. Ohnishi and T. Ohnishi, *Membrane Abnormalities in Sickle Cell Disease and in Other Red Blood Cell Disorders,* CRC Press, Boca Raton, Florida, 1994.
26. J. Harkness, *Biorheology*, 1971, **8**, 171-193.
27. M. J. Stutts, C. M. Canessa, J. C. Olsen, M. Hamrick, J. A. Cohn, B. C. Rossier and R. C. Boucher, *Science*, 1995, **269**, 847-850.
28. P. M. Moriarty and C. A. Gibson, *Cardiovasc. Rev. Rep.*, 2003, **24**, 321-325.
29. S. Alain, G. Jérôme, C. Gilles, M. Jean-Louis and L. Jaime, *J. Hypertens.*, 2002, **20**, 159-169.
30. I. Uchimura and F. Numano, *Diabetes Front.*, 1997, **8**, 33-37.
31. R. O. Loutfy and B. A. Arnold, *J. Phys. Chem.*, 1982, **86**, 4205-4211.
32. M. A. Haidekker, T. T. Ling, M. Anglo, H. Y. Stevens, J. A. Frangos and E. A. Theodorakis, *Chemistry & Biology*, 2001, **8**, 123-131.
33. B. D. Allen, A. C. Benniston, A. Harriman, S. A. Rostron and C. Yu, *Phys. Chem. Chem. Phys.*, 2005, **7**, 3035-3040.
34. M. A. H. Alamiry, A. C. Benniston, G. Copley, K. J. Elliott, A. Harriman, B. Stewart and Y. G. Zhi, *Chem. Mater.*, 2008, **20**, 4024-4032.
35. X. Yin, Y. Li, Y. Zhu, X. Jing, Y. Li and D. Zhu, *Dalton Trans.*, 2010, **39**, 9929-9935.
36. F. Zhou, J. Shao, Y. Yang, J. Zhao, H. Guo, X. Li, S. Ji and Z. Zhang, *Eur. J. Org. Chem.*, 2011, 4773-4787.
37. H. S. Guo, P. Zhu, F. Guo, X. L. Li, X. L. Wu, X. Y. Fan, L. Wen and F. C. Tang, *Nature Protocols*, 2015, **10**, 645-659.
38. F. Liu, T. Wu, J. Cao, S. Cui, Z. Yang, X. Qiang, S. Sun, F. Song, J. Fan, J. Wang and X. Peng, *Chem. Eur. J.*, 2013, **19**, 1548-1553.
39. D. Fischer, E. A. Theodorakis and M. A. Haidekker, *Nat. Protoc.*, 2007, **2**, 227-236.
40. X. Peng, Z. Yang, J. Wang, J. Fan, Y. He, F. Song, B. Wang, S.

Sun, J. Qu, J. Qi and M. Yan, *J. Am. Chem. Soc.*, 2011, **133**, 6626-6635.
41. Z. Yang, J. Cao, Y. He, J. H. Yang, T. Kim, X. Peng and J. S. Kim, *Chem. Soc. Rev.*, 2014, **43**, 4563-4601.
42. M. A. Haidekker, T. P. Brady, D. Lichlyter and E. A. Theodorakis, *Bioorg. Chem.*, 2005, **33**, 415-425.
43. Th. Förster and Z. G. Z. Hoffmann, *Phys. Chem.* , 1971, **75**, 63-76.
44. B. J. Coe, J. A. Harris, I. Asselberghs, K. Wostyn, K. Clays, A. Persoons, B. S. Brunschwig, S. J. Coles, T. Gelbrich, M. E. Light, M. B. Hursthouse and K. Nakatani, *Adv. Funct. Mater.*, 2003, **13**, 347-357.
45. G. S. He, J. Zhu, A. Baev, M. Samoc, D. L. Frattarelli, N. Watanabe, A. Facchetti, H. Agren, T. J. Marks and P. N. Prasad, *J. Am. Chem. Soc.*, 2011, **133**, 6675-6680.
46. Q. Zheng, H. Zhu, S. C. Chen, C. Tang, E. Ma and X. Chen, *Nature Photonics*, 2013, **7**, 234-239.
47. M. R. Gill, J. Garcia-Lara, S. J. Foster, C. Smythe, G. Battaglia and J. A. Thomas, *Nat. Chem.*, 2009, **1**, 662-667.
48. X. Wang, X. Tian, Q. Zhang, P. Sun, J. Wu, H. Zhou, B. Jin, J. Yang, S. Zhang, C. Wang, X. Tao, M. Jiang and Y. Tian, *Chem. Mater.*, 2012, **24**, 954-961.
49. R. Indumathy, S. Radhika, M. Kanthimathi, T. Weyhermuller and B. Unni Nair, *J. Inorg. Biochem.*, 2007, **101**, 434-443.
50. B. Zhou, W. Liu, H. Zhang, J. Wu, S. Liu, H. Xu and P. Wang, *Biosens. Bioelectron.*, 2015, **68**, 189-196.
51. G. Song, Y. Sun, Y. Liu, X. Wang, M. Chen, F. Miao, W. Zhang, X. Yu and J. Jin, *Biomaterials*, 2014, **35**, 2103-2112.
52. B. Dumat, G. Bordeau, A. I. Aranda, F. Mahuteau-Betzer, Y. El Harfouch, G. Metge, F. Charra, C. Fiorini-Debuisschert and M. P. Teulade-Fichou, *Org. Biomol. Chem.*, 2012, **10**, 6054-6061.
53. G. Wu, D. H. Robertson, C. L. Brooks III, M. Vieth, *J. Comp. Chem.* 2003, **24**, 1549-1562.
54. O. P. Cetinkol and N. V. Hud, *Nucleic Acids Res.*, 2009, **37**, 611-621.
55. Rangana Sinha and G. S. Kumar, *J. Phys. Chem. B* 2009, **113**, 13410-13420.